8478 *Biochemistry* **2010,** *49,* 8478–8487
DOI: 10.1021/bi100952k

BIOCHEMISTRY
including biophysical chemistry & molecular biology
Article

Defining a Stem Length-Dependent Binding Mechanism for the Cocaine-Binding Aptamer. A Combined NMR and Calorimetry Study[†]

Miguel A. D. Neves,[‡] Oren Reinstein, and Philip E. Johnson*

Department of Chemistry, York University, 4700 Keele Street, Toronto, Ontario, Canada M3J 1P3 [‡]*Current address: Department of Chemistry, University of Toronto, Toronto, Ontario, Canada*

Received June 14, 2010; Revised Manuscript Received August 22, 2010

ABSTRACT: We have used a combined approach of NMR spectroscopy and isothermal titration calorimetry (ITC) to determine the ligand-binding mechanism employed by a cocaine-binding aptamer. We found that the length of the stem containing the 3′ and 5′ termini determines the nature of the binding mechanism. When this stem is six base pairs long, the secondary structure of the aptamer is fully folded in the free form and only putative tertiary interactions form with ligand binding. If this stem is shortened by three base pairs, the free form of the aptamer contains little secondary structure, and ligand binding triggers secondary structure formation and folding. This binding mechanism is supported by both NMR spectral changes and the ITC measured heat capacity of binding ($\Delta C_p°$). For the aptamer with the long stem the $\Delta C_p°$ value is -557 ± 29 cal mol^{-1} K^{-1} and for the aptamer with the short stem the $\Delta C_p°$ value is -922 ± 51 cal mol^{-1} K^{-1}. Chemical shift perturbation data and the observation of intermolecular NOEs indicate that the three-way junction is the site of ligand binding.

The development of aptamers as biosensors is a rapidly developing area of biochemistry due to the ease of selecting aptamers and the ability of aptamers to bind virtually any ligand with high specificity (*1*, *2*). Nucleic acid aptamers are typically selected to bind their targets through an *in vitro* evolutionary selection process termed systematic evolution of ligands by exponential enrichment (SELEX) (*3*, *4*). This strategy can be employed to select for both RNA and DNA aptamers, although DNA aptamers may be preferable in applications used outside of the laboratory environment due to a greater resistance to degradation.

Despite their importance, the function of aptamers is often thought of as a black box, with few aptamers having their binding mechanism studied in detail. For many aptamers studied, and particularly for RNA aptamers, an adaptive binding mechanism has been proposed (*5*−*8*). In this mechanism, the free state of the aptamer or region of an aptamer exists in an unfolded or partially unfolded state, with the active state, or ligand-binding conformation, being just one of the many structures present in solution. In the presence of the correct ligand, the functional conformations in the unbound state bind the ligand, shifting the equilibrium to include more active states, which then go on to bind more ligand. This adaptive binding mechanism has been observed in the purine riboswitch (*9*). However, the generality of an adaptive binding mechanism in nucleic acid−small molecule interactions is unknown. For example, the lysine riboswitch regulatory element appears to present a prefolded structure, showing little conformation change with ligand binding (*10*).

Insights into the binding mechanism a biomolecule employs can come from a wide array of biophysical methods. NMR and X-ray crystallography studies give detailed structures of the free and bound states, but to date few structures exist detailing both the free and bound states of aptamers or other functional nucleic acids. Studies looking at the thermodynamics of ligand binding using calorimetric methods also yield important insights into ligand-binding mechanisms (*11*, *12*). These techniques have been used widely with protein−ligand systems (*13*−*15*) and are increasingly being employed in studying nucleic acid−small molecule interactions (*9*, *16*−*18*). Knowing the values of the thermodynamic binding parameters (ΔH, ΔS) derived from ITC studies as well as the change in heat capacity of binding (ΔC_p)[1] provides information on structural changes that occur with ligand binding.

One aptamer that has been the focus of a lot of development for use as a biosensor is the cocaine-binding DNA aptamer. The MNS-4.1 aptamer initially reported by Stojanovic et al. is highly selective for cocaine, with little affinity for common cocaine metabolites (*19*). The cocaine-binding aptamer is predicted to fold into three helical stems built around a three-way junction (Figure 1). Stem 2 contains only Watson−Crick base pairs, while stems 1 and 3 contain two putative noncanonical base pairs. In the unbound state, the cocaine-binding aptamer has been proposed to have one or more of the stems unfolded and only in the bound state do all three stems form (*20*).

Several biosensors for cocaine have been developed on the basis of the DNA sequence of this aptamer (*21*−*36*). The sensing technologies employing the cocaine-binding aptamer are varied and range from optical to electrochemical as well as spectroscopic. A number of the cocaine biosensors developed have exploited the binding-induced folding of the aptamer as a signaling trigger. This unfolded to folded transition is achieved by either shortening strand 1 by three base pairs or by dividing the aptamer into two separate strands. Only when in the presence of cocaine does this

[†]This work was supported by funding from the Natural Sciences and Engineering Research Council of Canada (NSERC) to P.E.J.

*Corresponding author. E-mail: pjohnson@yorku.ca. Phone: 416-736-2100 x3319. Fax: 416-736-5936.

[1]Abbreviations: bp, base pair; ΔC_p, change in heat capacity; K_d, dissociation constant; NMR, nuclear magnetic resonance; NOE, nuclear Overhauser effect; ITC, isothermal titration calorimetry.

 Published on Web 08/24/2010

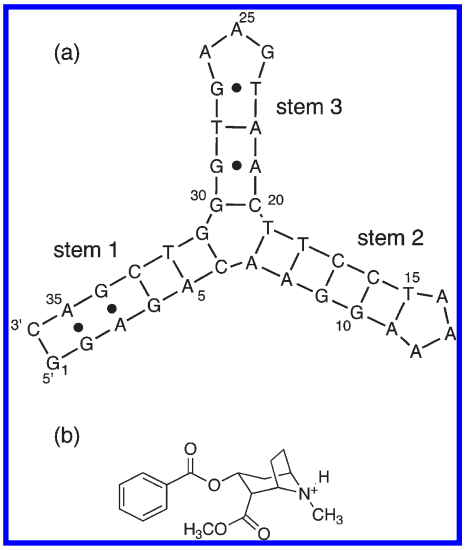

FIGURE 1: (a) Sequence of the MN1 cocaine-binding aptamer drawn with the originally proposed secondary structure. Dashes between nucleotides indicate Watson−Crick base pairs; dots indicate non-Watson−Crick base pairs. (b) Chemical structure of cocaine.

shortened aptamer fold, or the two strands come together, bind cocaine, and form the three-dimensional complex resulting in a signal (*19*, *27*, *29*, *33*, *34*). As an example of the versatility of the cocaine-binding aptamer, sequence variants have been adapted for use as a set, or array, of aptamers for hydrophobic molecules such as steroids (*37*, *38*). This resulted from the observation that a similarly structured three-way junction motif as predicted for the cocaine-binding aptamer had earlier been identified in a steroid-binding aptamer (*39*).

In this study we use NMR spectroscopy and isothermal titration calorimetry (ITC) to gain insight into the binding mechanism employed by the cocaine-binding aptamer. We find that two binding mechanisms are followed depending on the length of one of the stems. From changes in the NMR spectrum of the free and bound aptamer, from ITC derived measurement of the change in heat capacity of binding (ΔC_p), and from thermal stability measurements we determined the following: (i) when the stem that contains the 3′ and 5′ ends is short (three base pairs long), the aptamer undergoes a transition from an unstructured state with little secondary structure to a well-structured bound state; (ii) when the stem containing the 3′ and 5′ ends is six base pairs long, the aptamer is structured in the free state and retains the same secondary structure in the bound form. This limited structural change is in contrast to a previously proposed mechanism that suggested a significant amount of secondary structure forming with cocaine binding (*20*).

MATERIALS AND METHODS

Materials. Aptamer samples were obtained from the University of Calgary DNA Service. DNA samples for NMR analysis were purified by denaturing (8 M urea) 20% polyacrylamide gel electrophoresis. The DNA was separated from the gel by electroelution, and the DNA samples were pooled, exchanged three times in a 3 kDa molecular mass cutoff concentrator with sterilized 1 M NaCl, and subsequently washed at least three times with distilled deionized H_2O. DNA samples for ITC and UV−vis experiments were exchanged with 20 mM Tris (pH 7.4), 140 mM NaCl, and 5 mM KCl three times before use. Cocaine hydrochloride was obtained from Sigma-Aldrich.

NMR Spectroscopy. All 1D-^{1}H NMR experiments on aptamer samples were acquired using a 600 MHz Bruker Avance spectrometer. 2D NOESY (τ_m = 200 ms) spectra in $H_2O/^2H_2O$ (90%/10%) were recorded at 5 °C. A 2D NOESY (τ_m = 200 ms) and a TOCSY spectrum (*40*) (τ_m = 72 ms) were acquired on the MN4 aptamer in ^2H_2O at 20 °C using a Varian 800 MHz NMR spectrometer. Aptamer concentration for NMR studies ranged from 0.5 to 2.3 mM. Data were analyzed using CcpNmr Analysis (*41*).

Isothermal Titration Calorimetry. Isothermal titration calorimetry (ITC) was performed using a MicroCal VP-ITC instrument, and the data were analyzed using the accompanying Origin software fit to a one-site binding model. Samples were degassed before use with the MicroCal Thermo Vac unit. All experiments were corrected for the heat of dilution of the titrant. Unless otherwise specified, cocaine and aptamer solutions were prepared in a buffer of 20 mM Tris (pH 7.4), 140 mM NaCl, and 5 mM KCl. Binding experiments were typically performed with aptamer solutions of 20 μM using cocaine concentrations of 280 μM at 20 °C. All aptamer samples were heated in a boiling water bath for 3 min and cooled on ice prior to use in a binding experiment to allow the aptamer to anneal. Binding experiments consisted of (1) 30 successive 8 μL injections of cocaine every 300 s to a final molar ratio of 2.5:1 or (2) 36 injections of 6 μL of cocaine spaced every 300 s with a first injection of 1 μL to a final molar ratio of 2:1.

A low c ITC method was developed for use with the weaker binding constructs or conditions (*42*, *43*). For low c ITC experiments the running conditions were kept the same; however, these experiments consisted of 35 successive injections of a 45 mM cocaine solution. The first 10 injections were 5 μL, and the remaining additions were 8 μL injected every 300 s to a 50-fold molar excess of cocaine. The raw low c data were also corrected for heat of dilution of the titrant. The constructs fit under these low c conditions are MN6 and MN19.

Determination of the Isobaric Heat Capacity of Binding. The isobaric heat capacity (ΔC_p) of cocaine binding for MN4 and MN6 was determined by measuring the thermodynamics of binding over a temperature range of 5−50 °C with an aptamer solution of 20 μM and a cocaine solution of 3.6 mM in a buffer of 20 mM Tris (pH 7.4), 140 mM NaCl, and 5 mM KCl. The ITC experiments conducted to measure the thermodynamic parameters consisted of 35 successive injections of cocaine spaced every 300 s. The first injection was 1 μL followed by 20 injections of 3 μL and 14 injections of 15 μL to ensure complete binding site saturation. These low c conditions were selected so that all temperatures could be studied using the same experimental parameters. Since all experiments were allowed to reach complete binding site saturation, the observed saturation was used as the dilution reference (*44*). The $\Delta C_p°$ was determined by fitting the ITC measured enthalpy and free energy to the equations:

$$\Delta G = \Delta G° + T\int_{\tau°}^{\tau} \Delta H \, d\tau \quad (1)$$

$$\Delta H = \Delta H° + \int_{T°}^{T} \Delta C_p \, dT \quad (2)$$

$$\Delta C_p = \Delta C_p° + \Delta\varphi_p(T - T°) \quad (3)$$

Here ΔG and ΔH are the free energy and enthalpy at the given temperature, $\Delta G°$ and $\Delta H°$ are the free energy and enthalpy at

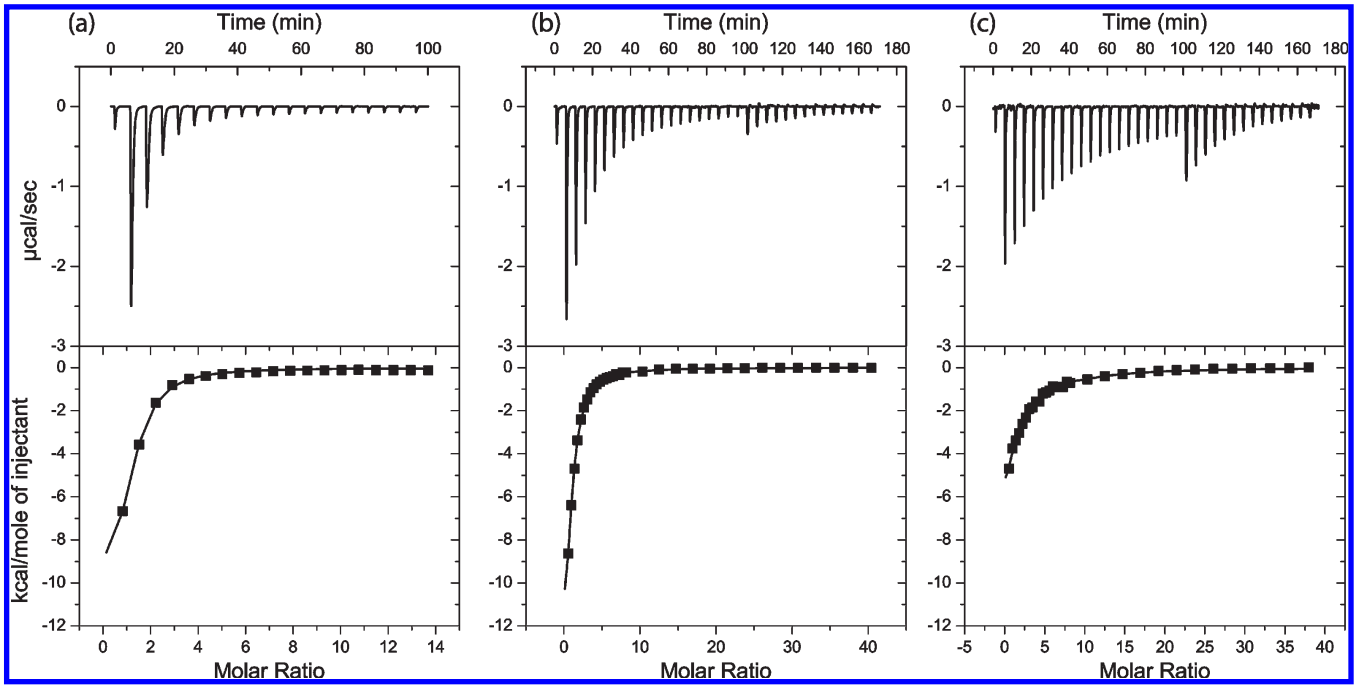

FIGURE 2: ITC analysis of cocaine binding by the MN4 aptamer at different temperatures. Shown are the titrations of cocaine into an MN4 aptamer solution at (a) 10, (b) 25, and (c) 50 °C. On top is the raw titration data showing the heat resulting from each injection of cocaine into an aptamer solution. On the bottom are the integrated heats after correcting for the heat of dilution. Binding experiments were performed in 20 mM Tris (pH 7.4), 140 mM NaCl, and 5 mM KCl.

standard conditions, $(T - T°)$ is the change in temperature, $\tau = 1/T$, and $\Delta\varphi_p$ is a term that represents the linear change in the heat capacity (*9*). Under circumstances where $\Delta\varphi_p$ is small, the enthalpy versus temperature curve can be fit linearly to eq 4. Linear regression analysis of the data fit yields the values of $\Delta C_p°$ and $\Delta H°$ as well as the associated errors.

$$\Delta H = \Delta H° + \Delta C_p(T - T°) \quad (4)$$

Surface Area Calculations. In order to determine the polar and nonpolar surface area of cocaine, a PDB file of the molecule was generated using PRODRG (*45*). The amount of polar and apolar area was then determined using the VEGA WE online server (*46*). The expected ΔC_p based on the change in polar (ΔA_p) and apolar (ΔA_{np}) surface area was calculated using the method of Spolar and Record, where $\Delta C_p = (0.32 \pm 0.04)\Delta A_{np} - (0.14 \pm 0.04)\Delta A_p$ (cal mol^{-1} K^{-1}) (*47*).

UV−Vis Spectroscopy. Temperature-dependent UV absorption experiments were recorded on a Cary BIO 100 spectrometer equipped with a 6 × 6 thermoelectrically controlled cell holder. Absorption of the DNA was monitored at 260 nm with the aptamer in the same buffer used for the ITC and NMR experiments. The concentration of the aptamer was 4 μM. For the melts of the bound aptamer, the ITC-determined dissociation constant was used to calculate the amount of ligand needed to result in 95% of the aptamer being bound. The temperature was raised at 0.5 °C min^{-1}; samples were allowed to equilibrate for 5 min prior to the start of the experiment. Data were plotted as the fractional increase in absorbance relative to the initial absorbance at 20 °C.

RESULTS

Affinity of Cocaine Binding by Aptamer Variants. Isothermal titration calorimetry was used to quantify the ligand-binding affinity and thermodynamics of the cocaine-binding aptamer and a set of sequence variants (Figure 2, Table 1). Two sets of aptamers were analyzed, those with a long stem 1 (6 bp, MN1 and MN4, Figure 3) and aptamers with a shortened stem 1 (3 bp, MN6 and MN19, Figure 3). Both sets of aptamers bind cocaine. The aptamers with a full-length stem 1 have tighter binding. In both pairs of aptamers, the change of a GT base pair to a GC base pair in stem 3 results in significantly tighter binding. For all aptamers binding is enthalpically driven and entropically unfavorable under all of the conditions studied (Table 1, Figure 1 of the Supporting Information).

Table 1: Dissociation Constant and Thermodynamic Parameters of Cocaine Binding for the Aptamers Presented in This Study[a]

aptamer	K_d (μM)	ΔH (kcal mol^{-1})	$-T\Delta S$ (kcal mol^{-1})
MN1	9.15 ± 0.09	−28.1 ± 0.7	21.1 ± 0.7
MN4	7 ± 1	−14.5 ± 0.4	7.6 ± 0.5
MN6	45.3 ± 0.5	−22.3 ± 1.6	16.5 ± 1.6
MN19	26.7 ± 0.7	−23.9 ± 0.9	17.7 ± 0.9

[a]Data acquired at 20 °C in 20 mM Tris (pH 7.4), 140 mM NaCl, and 5 mM KCl. The values reported are averages of two to four individual experiments. The error range reported is one standard deviation.

Change in Heat Capacity for Cocaine Binding. The $\Delta C_p°$ for cocaine binding by MN4 was determined by measuring the enthalpy of binding at different temperatures over a temperature range of 10−50 °C (Figure 4). A complete table of ΔH and calculated ΔC_p values for all ITC experiments for MN4 is provided in Table S1 of the Supporting Information. From a fit of the MN4 data to an equation that accounts for a temperature-dependent heat capacity change, we determined $\Delta C_p°$ to be −558.8 cal mol^{-1} K^{-1}. Additionally, the value of $\Delta\varphi_p$ was determined to be 0.251 cal mol^{-1} K^{-2}, and $\Delta H°$ was determined to be −19.4 kcal mol^{-1}. As the $\Delta\varphi_p$ value is small, it is possible to use a linear approximation to determine the value of $\Delta C_p°$ to be −557 ± 29 cal mol^{-1} K^{-1} and $\Delta H°$ to be −19 ± 1 kcal mol^{-1}.

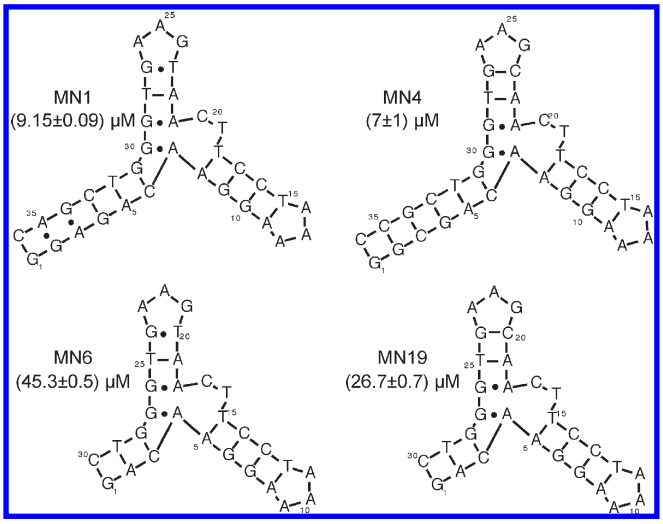

FIGURE 3: Secondary structure of the MN1, MN4, MN6, and MN19 aptamers drawn using the secondary structure presented here that contains the tandem GA mismatch. Also shown are the K_d values for each aptamer for cocaine determined at 20 °C in the buffer conditions 20 mM Tris (pH 7.4), 140 mM NaCl, and 5 mM KCl.

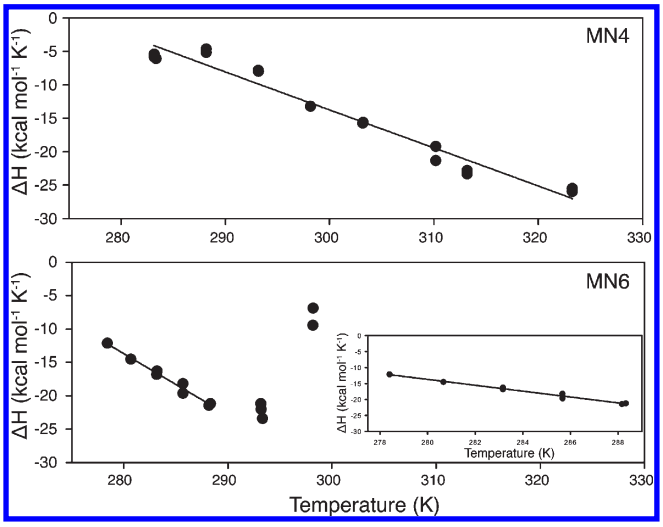

FIGURE 4: Temperature dependence of the enthalpy of cocaine binding for the MN4 and MN6 aptamers derived by ITC. The data values are shown as filled circles while the fit of the data to an equation that accounts for a temperature-dependent heat capacity change is the solid line. For MN6 only the low-temperature region where effects of aptamer unfolding do not contribute to the enthalpy was used in the fit (inset). Binding experiments were performed in 20 mM Tris (pH 7.4), 140 mM NaCl, and 5 mM KCl.

For MN6, the measured enthalpy data from 5 to 25 °C results from two effects: (1) binding of ligand and (2) folding of the aptamer. At low temperatures (5−15 °C) folding of the aptamer is complete, and these effects result in a near linear fit of the enthalpy to the heat capacity equations to result in a $\Delta C_p°$ of −918.6 cal mol^{-1} K^{-1}, a value of $\Delta\varphi_p$ of 1.6 cal mol^{-1} K^{-2}, and $\Delta H°$ was determined to be −33.4 kcal mol^{-1}. As for MN4, the value of $\Delta\varphi_p$ for MN6 is very small. When the data were fit to the linear approximation, the value of $\Delta C_p°$ is determined to be -922 ± 51 cal mol^{-1} K^{-1} and $\Delta H°$ to be -30 ± 2 kcal mol^{-1}. At temperatures above 15 °C, binding of ligand does not result in 100% folding of the aptamer. As temperature rises, an increasing percentage of the aptamer remains unfolded in the presence of ligand. This means less of the enthalpy of folding is added to the enthalpy of binding, resulting in a trend to larger (less negative) enthalpy values at temperatures over 15 °C. Consequently, the data acquired at 20 and 25 °C were not used in the data fitting to determine $\Delta C_p°$. A table of ΔH and calculated ΔC_p values for all ITC experiments for MN6 is provided in Table S2 of the Supporting Information.

NMR Assignments and Secondary Structure. NMR spectroscopy was used to analyze the stability and binding ability of the cocaine-binding aptamer as well as provide structural information about the cocaine-binding aptamers used in this study. As a first step to a detailed structural study, the imino resonances of the aptamers were assigned using two-dimensional NMR methods. The 1D-^{1}H NMR spectrum of MN1 was initially promising as it showed roughly the expected number of resonances for a molecule with 14 base pairs (Figure 5). This indicated that all three stems are fully formed in MN1 even in the absence of ligand. However, spectra of 2D NMR experiments on MN1 were uniformly very poor, with few cross-peaks visible. Upon the addition of cocaine, many resonances in MN1 change chemical shift and the peaks become sharper, but roughly the same number of resonances are observed. The 2D NMR experiments of cocaine-bound MN1 were still poor, and only partial assignments of the cocaine-bound conformation were obtained (Figure 5). In contrast to MN1, the MN4 aptamer provided good quality NMR spectra. In the cocaine-free conformation the imino region of the ^{1}H NMR spectrum of MN4, like MN1, contained the expected number of peaks for the number of base pairs, but the peaks in MN4 were much sharper than for free MN1 (Figure 5). With cocaine binding a number of peaks changed chemical shift, and the sharpness of the peaks from MN4 increased further (Figure 5).

Assignments of the imino resonances in the unbound and cocaine-bound MN4 aptamer were readily obtained from 2D NOESY spectra of the aptamer in water (Figure 6a). Complete assignments of the imino resonances of cocaine-bound MN4 were obtained with the exception of G1. The resonance from G1 is likely not present due to stem breathing motions as G1 is in the first base pair and is found at the base of stem 1. The three stems of MN4 each show a series of NOEs connecting adjacent base pairs (Figure 6a), but no interstem NOEs are observed, suggesting that there are no base stacking interactions or close contact between base pairs across the junction. Additionally, in the cocaine-free spectrum of MN4 (Figure 5 and Figure 2 of the Supporting Information) the imino resonance of T19 is not observed but is seen in the bound spectrum as the most downfield resonance.

One feature immediately apparent in the imino region of the spectrum of the MN4 cocaine-binding aptamer is the presence of one weak and two strong upfield signals around 10.5 ppm (Figures 5b and 6a). The weak peak is assigned to G24 in the triloop of stem 3. The two strong resonances show an NOE between them in the 2D NOESY (Figure 6a). The upfield nature of these imino resonances indicates they do not arise from standard Watson−Crick base pairs but are in a chemical shift range typical for sheared GA base pairs (*48*−*52*). From the original secondary structure prediction (Figure 1) we can expect that one imino peak is from a GA base pair, and the most likely conclusion is that there are two adjacent GA base pairs in MN4 as shown in Figure 3. Consistent with our proposed secondary structure for the cocaine-binding aptamer, the 1D-^{1}H NMR spectrum of the imino region of a construct (WC) where all of the non-Watson−Crick base pairs in the original secondary structure were changed to be Watson−Crick base pairs still shows the

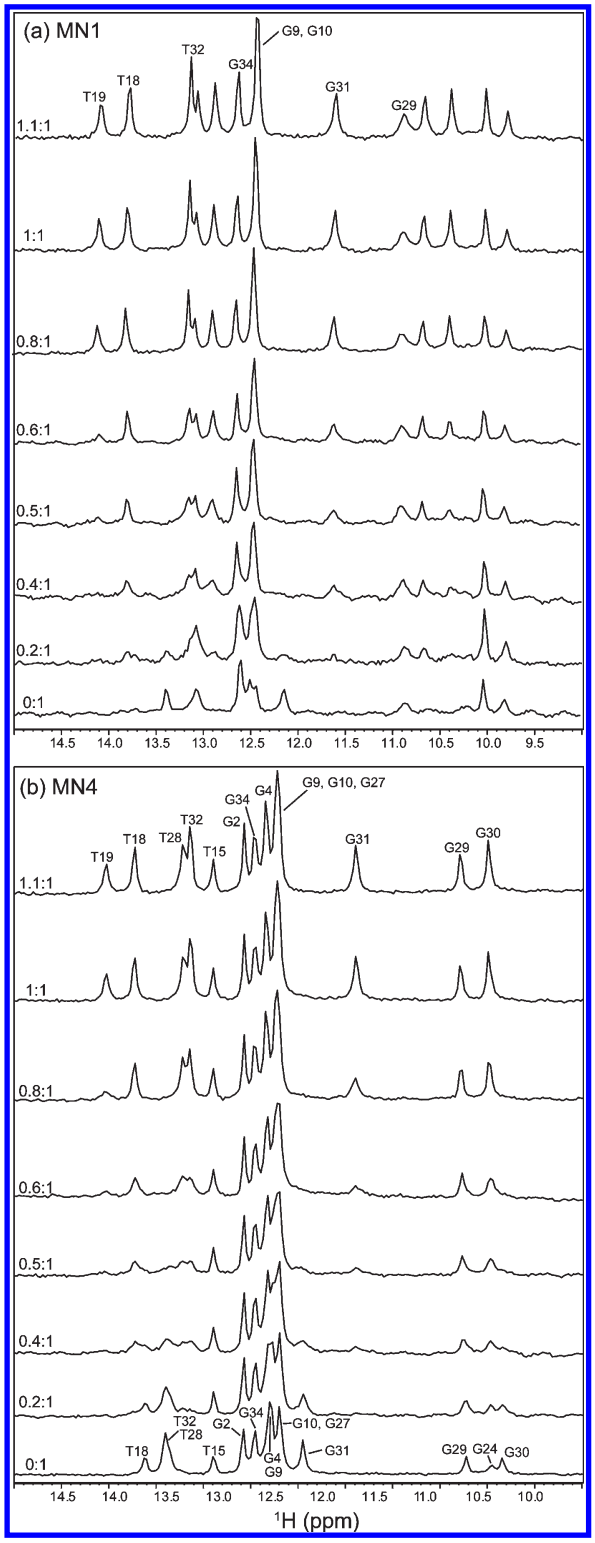

FIGURE 5: Cocaine binding by the (a) MN1 and (b) MN4 aptamers monitored by 1D-^{1}H NMR spectra. Shown is the region of the NMR spectrum focusing on the imino resonances as a function of increasing cocaine concentration. For MN4 the assignments are indicated; for MN1 only partial assignments of the bound spectrum were obtainable. Spectra were acquired in 90% H_2O/10% ^2H_2O at 5 °C. The molar ratios of cocaine:aptamer are indicated.

presence of a GA base pair in addition to the signal from G24 (Figure 3 of the Supporting Information). Additional NMR-based support for the presence of a sheared GA base pair is the observation of an NOE between the imino proton of G29 and the H8 proton of A21.

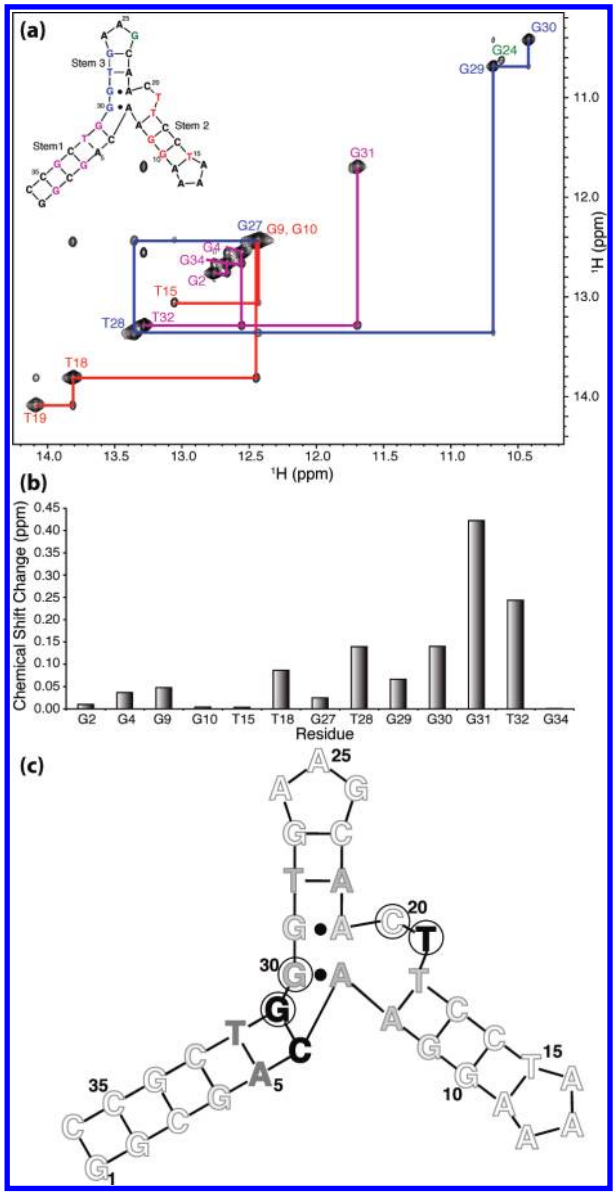

FIGURE 6: Imino proton assignments and change in imino chemical shift with cocaine binding. (a) Imino−imino region of the 2D NOESY (τ_m = 200 ms) of cocaine-bound NM4 in $H_2O/^2H_2O$ (90%/10%) recorded at 5 °C. Assignments are labeled in the spectrum and color coded according to their location in the structure. (b) Histogram showing the chemical shift perturbations of MN4 represented in terms of $\Delta\delta^1$H versus location in MN4. (c) Chemical shift perturbations mapped onto the secondary structure of the cocaine aptamer. The residues that move most are shown in shades of gray, with the residues that move the most shown in black and those that do not shift shown in white. T19, which is only observable in the cocaine-bound conformation, is also shown in black. Nucleotides that are circled show intermolecular NOEs to the aromatic ring on cocaine.

Insight into the location of the cocaine-binding site in the MN4 aptamer was gained by looking at the chemical shift perturbation upon ligand binding and the observation of intermolecular NOEs between the aptamer and the ligand. Panels b and c of Figure 6 summarize the chemical shift differences of the imino protons of MN4 between the free and cocaine-bound forms. The largest chemical shift perturbations were, in descending order, observed for G31, T32, G30, T28, and T18. All of these nucleotides are located at, or close to, the three-way junction (Figure 6c). Though the NMR resonances of the complex between MN4 and cocaine have not been fully assigned, the resonances of the aromatic ring

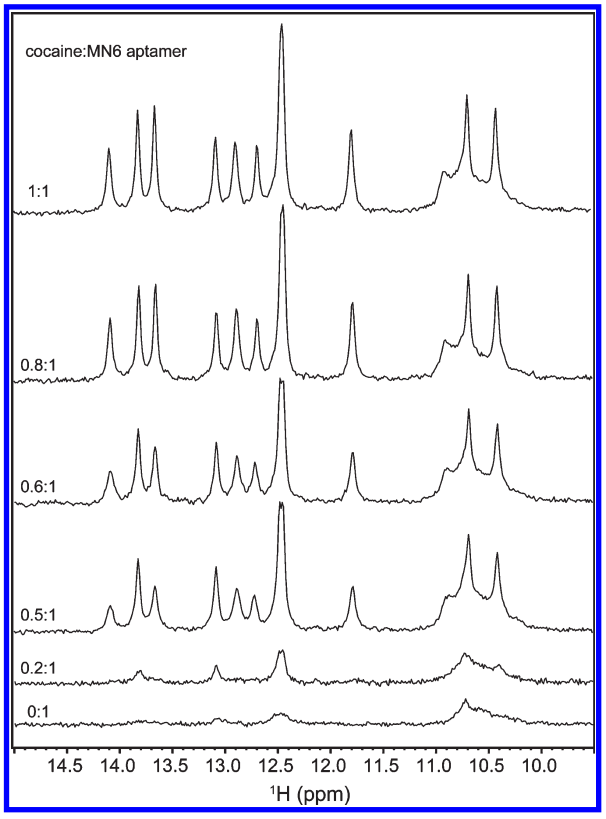

FIGURE 7: Cocaine binding by the MN6 aptamer monitored by 1D-^{1}H NMR spectra. Shown is the region of the NMR spectrum focusing on the imino resonances as a function of increasing cocaine concentration. In the absence of ligand the spectrum shows only a few very broad peaks indicative of little or no secondary structure being present. Upon binding ligand peaks from the folded cocaine-bound aptamer appear. Spectra were acquired in 90% H_2O/10% ^2H_2O at 5 °C. The molar ratios of cocaine:aptamer are indicated.

in cocaine (Figure 1b) are assigned. We have detected NOEs between the aromatic ring of cocaine and C20 H5, C20 H6, T19 H1′, T19 H2′, T19 H2″, T19 methyl, G30 H1′, G31 H1′, and G31 H8 (Figure 6c). Again, as all of these nucleotides are at the three-way junction, this implies that ligand binding occurs at the junction.

For the two aptamers with the short stem 1, MN6 and MN19, the NMR spectrum of the free aptamer showed only a few very weak and very broad peaks in the imino region (Figure 7 and Figure 4 of the Supporting Information). The spectra of the free MN6 and MN19 aptamers are indicative of very little to no secondary structure being present. With the addition of cocaine, the 1D-^{1}H NMR spectra of MN6 and MN19 dramatically change as numerous sharp peaks appear as the aptamer folds into a well-defined structure. The number of peaks in the bound spectrum of each aptamer is consistent with the number of base pairs expected in the secondary structure of the aptamers as shown in Figure 3.

Thermal Stability Analysis of the Cocaine-Binding Aptamers. The thermal stability of the MN1 and MN4 aptamers, both free and cocaine-bound, were assayed by UV−vis thermal melts. The midpoint temperature of unfolding of ligand-free MN1 is 41.1 °C rising to 45.2 °C when cocaine-bound (Figure 8). The MN4 aptamer is significantly more stable than MN1, having a midpoint temperature of unfolding of 57.0 °C for the ligand-free form and 61.0 °C for the ligand-bound aptamers. It is noteworthy that for both aptamers the difference in melt temperature for the free and bound form is very similar. The

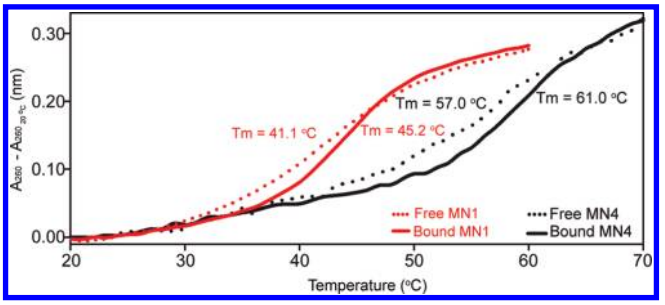

FIGURE 8: UV−vis melt profile of free and cocaine-bound MN1 and MN4 aptamers. The UV−vis melt profile was measured at 260 nm with the aptamers in 20 mM Tris (pH 7.4), 140 mM NaCl, and 5 mM KCl. For the cocaine-bound melts, sufficient cocaine was added to result in 95% of the aptamer being bound.

bound MN1 aptamer is 4.1 °C more stable than the free form, while the MN4 aptamer is 4.0 °C more stable.

The thermal stability of all four aptamers was also analyzed by following the intensity of peaks in the 1D-^{1}H NMR spectrum of the imino region of each aptamer with increasing temperature (Figure 9 and Figures 5 and 6 of the Supporting Information). For the free MN4 aptamer the last temperature at which an imino signal is visible is 35 °C, while for the bound aptamer this temperature increases to 40 °C. For the free MN1 aptamer the last temperature with an imino signal observable is 30 °C. For the cocaine-bound MN1 aptamer this increases to 35 °C (Figure 5 of the Supporting Information). For MN6 the last temperature at which the well-dispersed imino signals, indicative of a folded structure, are visible is at 15 °C (Figure 9). Similarly, for MN19 the temperature at which the well-dispersed imino signals disappear is at 15 °C (Figure 6 of the Supporting Information).

DISCUSSION

One goal of our research on the cocaine-binding aptamer is to define the structure of the complex using NMR methods. Initial NMR studies on MN1 yielded only very poor quality spectra. In order to improve the NMR spectrum of the cocaine-binding aptamer, we substituted some of the predicted noncanonical base pairs in MN1 with Watson−Crick base pairs to obtain the aptamer MN4 (Figure 3). Replacing three noncanonical base pairs in MN1 with Watson−Crick base pairs resulted in an aptamer with an increased affinity for cocaine (9.15 ± 0.09 μM for MN1 and 7 ± 1 μM for MN4) and which also displayed high-quality NMR spectra (Figures 5 and 6). Making changes to the three noncanonical base pairs indicates that the nucleotide identities at these positions (Figure 3) are not critical for ligand binding. Additionally, both the MN1 and MN4 aptamers have an enthalpically driven binding mechanism compensated by an unfavorable entropy of binding; this likely reflects a similar binding mechanism takes place for both aptamers. We also made similar changes in the aptamers with the short stem 1, changing the GT noncanonical base pair in stem 3 in MN6 to be a Watson−Crick GC in MN19. This single change significantly increased the affinity of the aptamer for cocaine from 45.3 ± 0.5 μM to 26.5 ± 0.5 μM and demonstrates the importance of having a Watson−Crick base pair at this position to achieve maximal affinity, affinity higher than the originally selected aptamer.

Secondary Structure of the Cocaine-Binding Aptamer. On the basis of the NMR assignments of MN4 we propose a secondary structure for the cocaine-binding aptamer that contains adjacent GA base pairs (Figure 3). Additional evidence for

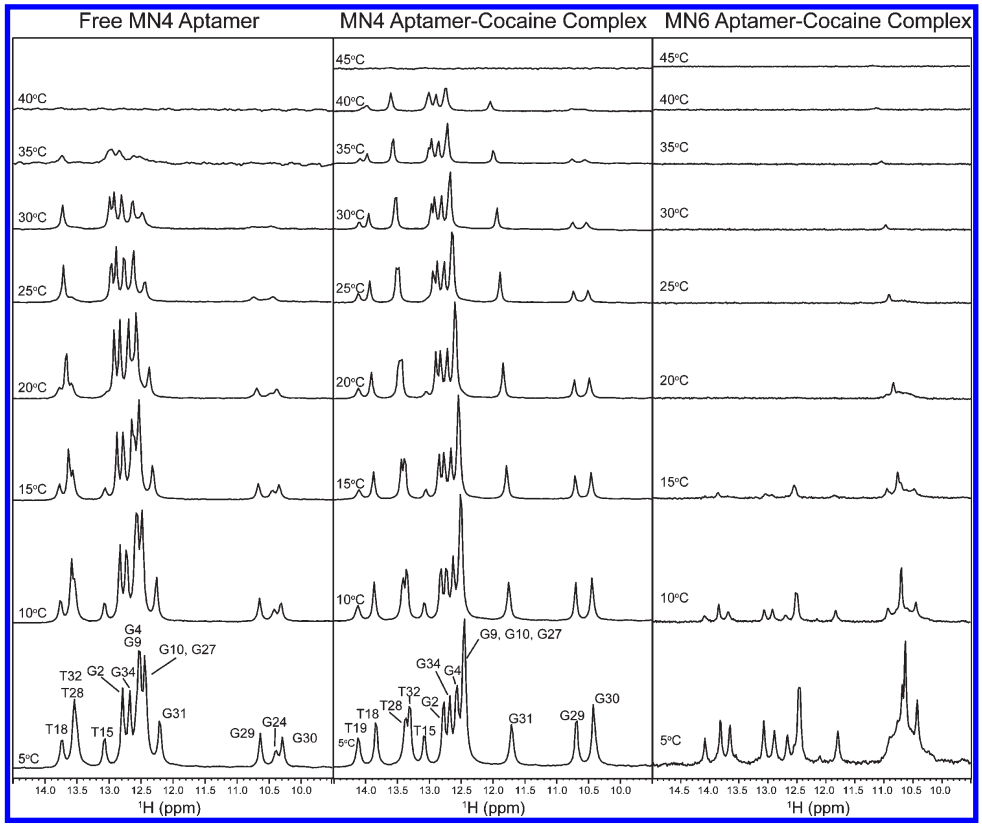

FIGURE 9: Thermal stability of the free and cocaine-bound MN4 and the bound MN6 aptamer measured by 1D-^{1}H NMR spectra. Shown is the region of the NMR spectrum focusing on the imino resonances as a function of increasing temperature from 5 to 45 °C. The assignments are indicated. Spectra were acquired in 90% H_2O/10% ^2H_2O.

this arrangement comes from a construct where all of the non-canonical base pairs present in the originally proposed secondary structure (Figure 1) have their sequence changed so as to form Watson−Crick base pairs (Figure 3 of the Supporting Information). In the imino spectrum of this aptamer two upfield peaks are observed, one due to the G24 in the triloop of stem 3 and a single GA imino peak. The incorporation of a tandem GA into the cocaine-binding aptamer secondary structure is readily accomplished by having the nucleotides T19 and C20 in a bulge. This dinucleotide bulge is consistent with T19 only being observable in the presence of cocaine. Presumably, T19 directly contacts cocaine in the complex in such a way as to result in the imino proton of T19 being protected from exchange and becoming visible or the T19 imino proton becomes involved in a new interaction, such as a base triple, within the aptamer.

The tandem GA sequence we propose here is a stable and common motif in DNA structures (*53*−*55*). The tandem GA mismatch has been shown to be the most stable tandem DNA mismatch in the context of having a 5′-C and a 3′-G and, in fact, is more stable in this sequence context than the corresponding Watson−Crick AT base pairs (*56*). Tandem GA base pairs have been identified in eukaryotic centromeric DNA sequences and have been extensively structurally studied (*48*, *52*, *57*, *58*). In a crystal structure of a tandem GA pair the mismatch caused the B-form helix to kink toward the major groove side, and extensive interstrand base stacking was observed at the GA mismatch (*57*). In the cocaine-binding aptamer the tandem GA mismatch likely imparts a conformation in the DNA structure required for ligand binding.

A Stem 1 Length-Dependent Binding Mechanism. The binding mechanism employed by the cocaine-binding aptamer depends on the length of stem 1. When stem 1 is short, containing three base pairs, the aptamer employs an adaptive binding mechanism and transitions from an unfolded to a folded structure with ligand binding. Alternately, when stem 1 is long, containing six base pairs, the secondary structure of the aptamer is preformed, and ligand binding induces very little change in secondary structure (Figure 10). Here we present both NMR and ITC data to support of this stem length dependent binding mechanism.

The NMR spectra of the cocaine-binding aptamers clearly indicate a binding mechanism that is highly dependent on the length of stem 1. For MN1 and MN4 the free aptamer contains the correct number of imino peaks for its secondary structure (Figure 3) to be fully formed in the free form. Upon addition of ligand, the peaks in the NMR spectrum of both MN1 and MN4 sharpen and become more intense. However, only one new peak appears in the bound form of the aptamer that is not observed in the free form, that of T19. In contrast, for both MN6 and MN19 the ^{1}H NMR spectrum of the free aptamer (Figure 7 and Figure 4 of the Supporting Information) indicates these aptamers contain only a small amount of secondary structure, two or three base pairs being present at most. Upon addition of ligand, the NMR spectrum dramatically changes with numerous narrow peaks from the bound form of the aptamer appearing. These changes indicate the aptamer folds with binding, and we note that the number of peaks observed for the bound MN6 and MN19 is consistent with their secondary structure shown in Figures 3 and 10.

Additional evidence in support of the stem 1 length-dependent binding mechanism being followed by the cocaine-binding aptamer comes from measurements of the change in heat capacity

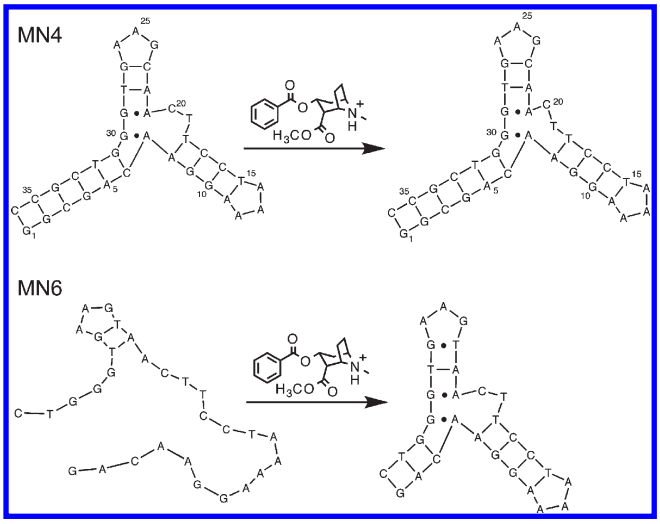

FIGURE 10: Proposed structural changes with ligand binding for the cocaine-binding aptamers with different lengths of stem 1. For aptamers with a long stem 1, such as for MN4, only tertiary structural changes are proposed to occur upon ligand binding. When stem 1 contains three base pairs, such as for MN6, the aptamer is unfolded when unbound and the secondary structure forms and the aptamer folds when the ligand is bound.

with ligand binding. For MN4, cocaine binding measurements at temperatures between 5 and 50 °C were used to determine the value of $\Delta C_p°$. From a fit of the temperature dependence of the binding enthalpy the value of $\Delta C_p°$ was determined to be -557 ± 29 cal mol^{-1} K^{-1}. Additionally, from fits of the data to eq 2, a value of $\Delta H°$ was determined to be -19 ± 1 kcal mol^{-1}. This value agrees within the error with the experimental value of -19.9 ± 0.5 kcal mol^{-1} (Table 1 of the Supporting Information). In contrast, binding data for MN6 acquired between 5 and 25 °C resulted in the determination of -922 ± 51 cal mol^{-1} K^{-1} for the $\Delta C_p°$ for this interaction. Measuring the $\Delta C_p°$ value is useful as this parameter is related to the change in polar and apolar surface area between the free ligand and macromolecule and the binary complex (*47*). For MN6, the greatly more negative value of $\Delta C_p°$ indicates a significantly larger amount of nonpolar surface area is buried than is seen with MN4 binding. This observation is consistent with a binding mechanism that involves folding of the macromolecule concurrent with ligand binding. If no structural change in the aptamer occurs with binding, the $\Delta C_p°$ value will reflect the extent of burial from solvent of the ligand. If cocaine is completely buried, the maximum negative value of -132.1 ± 21.0 cal mol^{-1} K^{-1} for $\Delta C_p°$ will occur. We attribute the difference in $\Delta C_p°$ between our experimental values for MN4 and MN6 and that from complete burial of cocaine to arise from structural changes in the aptamer upon binding. For MN4, as we see from the NMR data that little to no secondary structure change occurs with binding. Therefore, the structural change suggested by the $\Delta C_p°$ value likely reflects tertiary structure compaction. Such changes would be consistent with the improved NMR spectral quality of the bound versus the free aptamers. For MN6 the $\Delta C_p°$ of secondary structure formation is coupled to binding and gives rise to the much larger measured value.

Similar differences between the measured $\Delta C_p°$ and the expected $\Delta C_p°$ based on change in polar and nonpolar surface area have been previously observed in both small molecule–RNA and small molecule–DNA interactions (*9*, *17*, *18*, *59*). Our experimental values of $\Delta C_p°$ of -557 ± 29 cal mol^{-1} K^{-1} for MN4 and of -922 ± 51 cal mol^{-1} K^{-1} for MN6 lie in the high range reported for these other nucleic acid–small molecule systems. The previously most negative $\Delta C_p°$ value was -0.81 kcal mol^{-1} K^{-1} for the purine riboswitch aptamer domain (*9*), while the least negative was -116 cal mol^{-1} K^{-1} for the L-argininamide-binding DNA aptamer (*17*). While the value of $\Delta C_p°$ arises from numerous factors, it is likely that the larger negative magnitude of $\Delta C_p°$ tracks the amount of structural change with ligand binding for these systems.

Some of the applications of the cocaine-binding aptamer rely on an aptamer with the MN6 sequence transitioning from an unfolded to folded structure with ligand binding (*5*–*8*). This folding transition was also observed in a recent EPR and fluorescence study of the cocaine-binding aptamer (*60*). The authors proposed that stems 2 and 3 were formed prior to cocaine binding with stem 1 forming with binding. In contrast, we show that only two to three base pairs might be formed prior to ligand binding. For the aptamer with the long stem 1 an adaptive binding mechanism was previously proposed where stem 3 folds with cocaine binding (*20*). Here we show that all three stems are folded in the free state with only changes in the tertiary structure potentially taking place upon ligand binding.

The NMR and UV thermal melt data show that there is small (~4 °C) difference in thermal stability between the free and bound aptamer for both MN1 and MN4. This observation is consistent with our binding mechanism where there is little significant secondary structure formation with cocaine binding in both MN1 and MN4. In contrast to our small increase in T_m, the L-argininamide-binding DNA aptamer melt temperature increases by about 10 °C when ligand bound (*17*). In addition to the interactions to the ligand, the L-argininamide-binding aptamer becomes significantly more compact, and one or two base pairs form upon binding. The melt temperature for MN1 and MN4 increases by about half of this amount, and we expect the stabilization to arise from additional tertiary interactions or at most one additional base pair forming with ligand binding. For both MN6 and MN19 the ligand-bound forms are significantly less stable than MN1 and MN4. This is consistent with a fewer total number of base pairs being present in these aptamers. The NMR-monitored thermal melts show the well-dispersed signals from the folded MN6 and MN19 aptamers disappearing above 15 °C, indicating these aptamers are only marginally stable at room temperature.

There is a small and consistent difference between the melt temperature determined by UV and the last temperature at which an imino signal is observed. The intensity of an imino proton NMR signal decreases for two possible reasons. First, at temperatures above the melting temperature the base pair is unstructured, resulting in the disappearance of the imino signals. Second, as the temperature increases, the imino resonances exchange with water faster; this also diminishes the signal intensity. The disappearance of the imino signals approximately 5 °C lower than that determined by UV thermal melt likely reflects signal loss due to an increase in hydrogen exchange before complete unfolding of the DNA.

Thermodynamics of Ligand Binding. For all of the aptamers studied here, cocaine binding is an enthalpically driven process offset by an unfavorable entropic penalty. Two categories of DNA–small molecule binding interactions have been classified according to their thermodynamic signature. Groove binders display small negative or positive enthalpy with a favorable binding entropy, while intercalators have unfavorable entropy

and negative enthalpy values (*12*). The thermodynamic parameters we observe for MN1, MN4, MN6, and MN19 binding cocaine would put this interaction in the "intercalator" category. While we are not proposing that these aptamers follow a classic intercalation binding mechanism where the ligand sits between adjacent base pairs, we propose that the cocaine-binding aptamer follows a binding mechanism where the DNA rearranges to a more rigid structure. It is this rearrangement which gives rise to the thermodynamic signature of the intercalation mechanism (*12*). We note that this rearrangement is consistent with our large negative measured ΔC_p° values that suggest tertiary structure packing from MN1 and MN4.

We have used ITC methods to determine the energetics of cocaine binding for a series of DNA aptamers. This is the first study to look at the binding thermodynamics of the cocaine-binding aptamer, though previous studies have measured the binding affinities for some variants of the cocaine-binding aptamer. The affinities we report for MN1 are consistent with previously published binding data on the cocaine-binding aptamer. For the MN1 aptamer, we report a K_d of 9.15 ± 0.09 μM (Table 1); the MNS-4.1 aptamer was previously reported to have a K_d value of 0.4−10 μM in identical buffer and salt conditions (*21*). MN1 and MNS-4.1 are identical with the exception that MN1 is one base pair shorter as it does not have a terminal GA base pair in stem 1. This extra base pair in MNS-4.1 likely contributes little to cocaine binding. A cocaine-binding aptamer with the sequence of MN6 has been used in a number of previous studies (*21*, *27*). We report an affinity for the MN6 aptamer of 49 ± 1 μM, which is in line with the previous reports of 37 μM (*27*) and ~20 μM (*21*).

In summary, we present NMR and thermodynamic data to show that the cocaine-binding aptamer follows a stem length dependent binding mechanism. With a six base pair stem 1 the secondary structure of the aptamer is formed when free and ligand binding tightens up or orders the tertiary structure. When stem 1 has three base pairs, the aptamer is unfolded in the free state except for possibly two to three base pairs. Ligand binding induces secondary structure formation and folding of the bound aptamer. Our studies should provide guidance for the further development of anticocaine biosensors.

ACKNOWLEDGMENT

We thank Tara Sprules at the Québec/Eastern Canada High Field NMR facility (McGill University, Montreal, Canada) for performing the 800 MHz NMR experiments and members of the Johnson laboratory (York University, Toronto, Canada) and Wilce laboratory (Monash University, Clayton, Australia) for useful discussions.

SUPPORTING INFORMATION AVAILABLE

Tables of ΔH and ΔC_p values at different temperatures for MN4 and MN6 aptamers; figures of (1) temperature dependence of ΔH, $T\Delta S$, and ΔG for both MN4 and MN6, (2) the 2D NOESY showing the assignment of free MN4, (3) showing the 1D-^{1}H NMR spectrum of the WC construct providing evidence for the tandem GA base pairs, (4) showing the 1D-^{1}H NMR of the titration of cocaine into MN19, (5) showing the thermal melts of free and cocaine-bound MN1 monitored by 1D-^{1}H NMR, and (6) showing the thermal melt of cocaine-bound MN19 monitored by 1D-^{1}H NMR. This material is available free of charge via the Internet at http://pubs.acs.org.

REFERENCES

1. Bunka, D. H. J., and Stockley, P. G. (2006) Aptamers come of age—at last. *Nat. Rev. Microbiol. 4*, 588–596.
2. Mayer, G. (2009) The chemical biology of aptamers. *Angew. Chem., Int. Ed. 48*, 2672–2689.
3. Ellington, A. D., and Szostak, J. W. (1990) In vitro selection of RNA molecules that bind specific ligands. *Nature 346*, 818–822.
4. Tuerk, C., and Gold, L. (1990) Systematic evolution of ligands by exponential enrichment: RNA ligands to bacteriophage T4 DNA polymerasae. *Science 249*, 505–510.
5. Lin, C. H., and Patel, D. J. (1997) Structural basis of DNA folding and recognition in an AMP-DNA aptamer complex: distinct architectures but common recognition motifs for DNA and RNA aptamers complexed to AMP. *Chem. Biol. 4*, 817–832.
6. Williamson, J. R. (2000) Induced fit in RNA-protein recognition. *Nat. Struct. Biol. 7*, 834–837.
7. Leulliot, N., and Varani, G. (2001) Current topics in RNA-protein recognition: control of specificity and biological function through induced fit and conformational capture. *Biochemistry 40*, 7946–7956.
8. Latham, M. P., Zimmermann, G. R., and Pardi, A. (2009) NMR chemical exchange as a probe for ligand-binding kinetics in a theophylline-binding RNA aptamer. *J. Am. Chem. Soc. 131*, 5052–5053.
9. Gilbert, S. D., Stoddard, C. D., and Wise, S. J. (2006) Thermodynamic and kinetic characterization of ligand binding to the purine riboswitch aptamer domain. *J. Mol. Biol. 359*, 754–768.
10. Garst, A. D., Heroux, A., Rambo, R. P., and Batey, R. T. (2008) Crystal structure of the lysine riboswitch regulatory mRNA element. *J. Biol. Chem. 283*, 22347–22351.
11. Feig, A. L. (2007) Applications of isothermal titration calorimetry in RNA biochemistry and biophysics. *Biopolymers 87*, 293–301.
12. Chaires, J. B. (2008) Calorimetry and thermodynamics in drug design. *Annu. Rev. Biophys. 37*, 135–151.
13. Campoy, A. V., and Freire, E. (2005) ITC in the post-genomic era...? Priceless. *Biophys. Chem. 115*, 115–124.
14. Privalov, P. L., and Dragan, A. I. (2007) Microcalorimetry of biological macromolecules. *Biophys. Chem. 126*, 16–24.
15. Weber, P. C., and Salemme, F. R. (2003) Applications of calorimetric methods to drug discovery and the study of protein interactions. *Curr. Opin. Struct. Biol. 13*, 115–121.
16. Cowan, J. A., Ohyama, T., Wang, D., and Natarajan, K. (2000) Recognition of a cognate RNA aptamer by neomycin B: quantitative evaluation of hydrogen bonding and electrostatic interactions. *Nucleic Acids Res. 28*, 2935–2942.
17. Bishop, G. R., Ren, J., Polander, B. C., Jeanfreau, B. D., Trent, J. O., and Chaires, J. B. (2007) Energetic basis of molecular recognition in a DNA aptamer. *Biophys. Chem. 126*, 165–175.
18. Lin, P.-H., Yen, S.-L., Lin, M.-S., Chang, Y., Louis, S. R., Higuchi, A., and Chen, W.-Y. (2008) Microcalorimetrics studies of the thermodynamics and binding mechanism between L-tyrosinamide and aptamer. *J. Phys. Chem. B 2008*, 66665–66673.
19. Stojanovic, M. N., de Prada, P., and Landry, D. W. (2000) Fluorescent sensors based on aptamer self-assembly. *J. Am. Chem. Soc. 122*, 11547–11548.
20. Stojanovic, M. N., and Landry, D. W. (2002) Aptamer-based colorimetric probe for cocaine. *J. Am. Chem. Soc. 124*, 9678–9679.
21. Stojanovic, M. N., de Prada, P., and Landry, D. W. (2001) Aptamer-based folding fluorescent sensor for cocaine. *J. Am. Chem. Soc. 123*, 4928–4931.
22. Baker, B. R., Lai, R. Y., Wood, M. S., Doctor, E. H., Heeger, A. J., and Plaxco, K. W. (2006) An electronic, aptamer-based small-molecule sensor for the rapid, label-free detection of cocaine in adulterated samples and biological fluids. *J. Am. Chem. Soc. 128*, 3138–3139.
23. Liu, J., Mazumdar, D., and Lu, Y. (2006) A simple and sensitive "dipstick" test in serum based on lateral flow separation of aptamer-linked nanostructures. *Angew. Chem., Int. Ed. 45*, 7955–7959.
24. Liu, J., and Lu, Y. (2006) Fast colorimetric sensing of adenosine and cocaine based on a general sensor design involving aptamers and nanoparticles. *Angew. Chem., Int. Ed. 45*, 90–94.
25. Shlyahovsky, B., Li, D., Weizmann, Y., Nowarski, R., Kotler, M., and Willner, I. (2007) Spotlighting of cocaine by an autonomous aptamer-based machine. *J. Am. Chem. Soc. 129*, 3814–3815.
26. Liu, J., Lee, J. H., and Lu, Y. (2007) Quantum dot encoding of aptamer-linked nonostructures for one-pot simultaneous detection of multiple analytes. *Anal. Chem. 79*, 4120–4125.
27. Li, T., Li, B., and Dong, S. (2007) Adaptive recognition of small molecules by nucleic acid aptamers through a label-free approach. *Chem.—Eur. J. 13*, 6718–6723.
28. Elbaz, J., Shlyahovsky, B., Li, D., and Willner, I. (2008) Parallel analysis of two analytes in solutions or on surfaces by using a

bifunctional aptamer: applications for biosensing and logic gate operations. *ChemBioChem 9*, 232–239.
29. Zhang, J., Wang, L., Pan, D., Song, S., Boey, F. Y. C., Zhang, H., and Fan, C. (2008) Visual cocaine detection with gold nanoparticles and rationally engineered aptamer structures. *Small 4*, 1196–1200.
30. Chen, J., Jiang, J., Gao, X., Liu, G., Shen, G., and Yu, G. (2008) A new aptameric biosensor for cocaine based on surace-enhanced raman scattering spectroscopy. *Chem.—Eur. J. 14*, 8374–8382.
31. White, R. J., Phares, N., Lubin, A. A., Xiao, Y., and Plaxco, K. W. (2008) Optimization of electrochemical aptamer-based sensors via optimization of probe packing density and surface chemistry. *Langmuir 224*, 10513–10418.
32. Swensen, J. S., Xiao, Y., Ferguson, B. S., Lubin, A. A., Lai, R. Y., Heeger, A. J., Plaxco, K. W., and Soh, H. T. (2009) Continuous, real-time monitoring of cocaine in undiluted blood serum via a microfluidic, electrochemical aptamer-based sensor. *J. Am. Chem. Soc. 131*, 4262–4266.
33. Freeman, R., Li, Y., Tel-Vered, R., Sharon, E., Elbaz, J., and Willner, I. (2009) Self-assembly of supramolecular aptamer structures for optical or electrochemical sensing. *Analyst 134*, 653–656.
34. Freeman, R., Sharon, E., Tel-Vered, R., and Willner, I. (2009) Supramolecular cocaine-aptamer complexes activate biocatalytic cascades. *J. Am. Chem. Soc. 131*, 5028–5029.
35. Zhang, C.-Y., and Johnson, L. W. (2009) Single quantum-dot-based aptameric nanosensor for cocaine. *Anal. Chem. 81*, 3051–3055.
36. Madru, B., Chapuis-Hugon, F., Peyrin, E., and Pichon, V. (2009) Determination of cocaine in human plasma by selective solid-phase extraction using an aptamer-based sorbent. *Anal. Chem. 81*, 7081–7086.
37. Stojanovic, M. N., Green, E. G., Semova, S., Nikic, D. B., and Landry, D. W. (2003) Cross-reactive arrays based on three-way junctions. *J. Am. Chem. Soc. 125*, 6085–6089.
38. Green, E., Olah, M. J., Abramova, T., Williams, L. R., Stefanovic, D., Worgall, T., and Stojanovic, M. N. (2006) A rational approach to minimal high-resolution cross-reactive arrays. *J. Am. Chem. Soc. 128*, 15278–15282.
39. Kato, T., Yano, K., Ikebukuro, K., and Karube, I. (2000) Interaction of three-way DNA junctions with steroids. *Nucleic Acids Res. 28*, 1963–1968.
40. Griesinger, C., Otting, G., Wüthrich, K., and Ernst, R. R. (1988) Clean TOCSY for ^{1}H spin system identification in macromolecules. *J. Am. Chem. Soc. 110*, 7870–7872.
41. Vraken, W. F., Boucher, W., Stevens, T. J., Fogh, R. H., Pajon, A., Llinas, M., Ulrich, E. L., Markley, J. L., Ionides, J., and Laue, E. D. (2005) The CCPN data model for NMR spectroscopy: development of a software pipeline. *Proteins 59*, 687–696.
42. Turnbull, W. B., and Daranas, A. H. (2003) On the value of c: can low affinity systems be studied by isothermal titration calorimetry? *J. Am. Chem. Soc. 125*, 14859–14866.
43. Tellinghuisen, J. (2008) Isothermal titration calorimetry at very low c. *Anal. Biochem. 373*, 395–397.
44. Recht, M. I., Ryder, S. P., and Williamson, J. R. (2008) Monitoring assembly of ribonucleoprotein complexes by isothermal titration calorimetry, in Methods in Molecular Biology (Lin, R.-J., Ed.) pp 117—127, Humana Press, Totowa, NJ.
45. Schuttelkopf, A. W., and van Aalten, D. M. F. (2004) PRODRG: a tool for high-throughput crystallography of protein-ligand complexes. *Acta. Crystallogr., Sect. D D60*, 1355–1363.
46. Pedretti, A., Villa, L., and Vistoli, G. (2004) VEGA—An open platform to develop chemo-bio-informatics applications, using plug-in architecture and script programming. *J. Comput.-Aided Mol. Des. 18*, 167–173.
47. Spolar, R. S., and Record, M., Jr. (1994) Coupling of local folding to site-specific binding of proteins to DNA. *Science 263*, 777–784.
48. Lane, A., Martin, S. R., Ebel, S., and Brown, T. (1992) Solution conformation of a deoxynucleotide containing tandem GA mismatched base pairs and 3′-overhanging ends in d(GTGAACTT)$_2$. *Biochemistry 31*, 12087–12095.
49. Chou, S.-H., and Chin, K.-H. (2001) Solution structure of a DNA double helix incorporating four consecutive non-Watson-Crick base-pairs. *J. Mol. Biol. 312*, 769–781.
50. Cheng, J.-W., Chou, S.-H., and Reid, B. R. (1992) Base pairing geometry in GA mismatches depends entirely on the neighboring sequence. *J. Mol. Biol. 228*, 1037–1041.
51. Greene, K. L., Jones, R. L., Li, Y., Robinson, H., Wang, A. H.-L., Zon, G., and Wilson, W. D. (1994) Solution structure of a GA mismatch DNA sequence, d(CCATGAATGG)$_2$ determined by 2D NMR and structural refinement methods. *Biochemistry 33*, 1053–1062.
52. Li, Y., Zon, G., and Wilson, W. D. (1991) NMR and molecular modeling evidence for a GA mismatch base pair in a purine-rich DNA duplex. *Proc. Natl. Acad. Sci. U.S.A. 88*, 26–30.
53. Chou, S.-H., Chin, K.-H., and Wang, A. H.-L. (2003) Unusual DNA duplex and hairpin motifs. *Nucleic Acids Res. 31*, 2461–2474.
54. Ortiz-Lombardia, M., Cortes, A., Huertas, D., Eritja, R., and Azorin, F. (1998) Tandem 5′-GA:GA-3′ mismatches account for the high stability of the fold-back structures formed by the centromeric *Drosophila* dodeca-satellite. *J. Mol. Biol. 277*, 757–762.
55. Ebel, S., Lane, A., and Brown, T. (1992) Very stable mismatch duplexes: structural and thermodynamic studies on tandem GA mismatches in DNA. *Biochemistry 31*, 12083–12086.
56. Ke, S.-H., and Wartell, R. M. (1996) The termal stability of DNA fragments with tandem mismatches at a d(CXYG)d(CY′X′G) site. *Nucleic Acids Res. 24*, 707–712.
57. Gao, Y.-G., Robinson, H., Sanishvili, R., Joachimiak, A., and Wang, A. H.-L. (1999) Structure and recognition of sheared tandem GA base pairs associated with human centromere DNA equence at atomic resolution. *Biochemistry 38*, 16452–16460.
58. Chou, S.-H., Cheng, J.-W., Fedoroff, O., and Reid, B. R. (1994) DNA sequence GCGAATGAGC containing the human centromere core sequence GAAT forms a self-complementary duplex with sheared GA pairs in solution. *J. Mol. Biol. 241*, 467–479.
59. Pilch, D. S., Kaul, M., Barbieri, C. M., and Kerrigan, J. E. (2003) Thermodynamics of aminoglycoside-rRNA recognition. *Biopolymers 70*, 58–79.
60. Cekan, P., Jonsson, E. O., and Sigurdsson, S. T. (2009) Folding of the cocaine aptamer studied by EPR and fluorescence spectroscopies using the bifunctional spectroscopic probe Ç. *Nucleic Acids Res. 37*, 3990–3995.